Journal of Solid State Chemistry 199 (2013) 34–41

Contents lists available at SciVerse ScienceDirect

Journal of Solid State Chemistry

journal homepage: www.elsevier.com/locate/jssc

Influence of the network modifier on the characteristics of $MSnO_3$ (M=Sr and Ca) thin films synthesized by chemical solution deposition

M.C.F. Alves [a,b], R.M.M. Marinho [b], G.P. Casali [b], M. Siu-Li [c], S. Députier [a], M. Guilloux-Viry [a], A.G. Souza [b], E. Longo [d], I.T. Weber [e], I.M.G. Santos [b,*], V. Bouquet [a]

[a] Institut des Sciences Chimiques de Rennes, UMR 6226 CNRS/Université de Rennes 1, Campus de Beaulieu, Rennes cedex 35042, France
[b] LACOM/INCTMN, Department de Química, Universidade Federal da Paraíba, Campus I, João Pessoa, Paraíba CEP 58059-900, PB, Brazil
[c] IFSC, Universidade de São Paulo, CEP 13560-970, São Carlos, SP, Brazil
[d] LIEC/INCTMN, Instituto de Química, Universidade Estadual Paulista, CEP 14801-907, Araraquara, SP, Brazil
[e] LMC, Instituto de Química, Universidade de Brasília, CEP 70910-900, Brasília, DF, Brazil

ARTICLE INFO

Article history:
Received 19 July 2012
Received in revised form
30 October 2012
Accepted 18 November 2012
Available online 29 November 2012

Keywords:
Perovskite
Stannates
Chemical solution deposition
Polymeric precursor method
Epitaxial growth
Photoluminescence

ABSTRACT

$CaSnO_3$ and $SrSnO_3$ alkaline earth stannate thin films were prepared by chemical solution deposition using the polymeric precursor method on various single crystal substrates (R- and C-sapphire and 100-$SrTiO_3$) at different temperatures. The films were characterized by X-ray diffraction (θ–2θ, ω- and φ-scans), field emission scanning electron microscopy, atomic force microscopy, micro-Raman spectroscopy and photoluminescence. Epitaxial $SrSnO_3$ and $CaSnO_3$ thin films were obtained on $SrTiO_3$ with a high crystalline quality. The long-range symmetry promoted a short-range disorder which led to photoluminescence in the epitaxial films. In contrast, the films deposited on sapphire exhibited a random polycrystalline growth with no meaningful emission regardless of the substrate orientation. The network modifier (Ca or Sr) and the substrate (sapphire or $SrTiO_3$) influenced the crystallization process and/or the microstructure. Higher is the tilts of the SnO_6 octahedra, as in $CaSnO_3$, higher is the crystallization temperature, which changed also the nucleation/grain growth process.

1. Introduction

The alkaline-earth stannates ($MSnO_3$, M=Ca, Sr, Ba) present very attractive dielectric and semiconducting properties that favor their application in various areas such as humidity sensors, capacitors and heat-stable lithium-ion batteries [1–3]. These perovskite materials may exhibit a distorted cubic structure due to the octahedral tilting distortion which depends on the covalent character of the M cation. Indeed, the Sn–O–Sn angle, expected to be 180° for $BaSnO_3$, varies from 159° to 161° for $SrSnO_3$ and from 146° to 149° for $CaSnO_3$ [4,5], which leads to properties that can be tuned according to the M modifier cation.

The synthesis of these materials in thin film form is very attractive for integration and miniaturization of the devices. Whereas the preparation of $SrSnO_3$ and $CaSnO_3$ in bulk form has been reported using different methods such as solid-state reaction, sol–gel process, hydrothermal and polymeric precursor methods [4–11], few works have been reported on the synthesis of thin films. $SrSnO_3$ and Tb–Mg co-doped $CaSnO_3$ thin films have been synthesized using radio frequency (RF) sputtering [12,13]. $SrSnO_3$ has been deposited on MgO substrate and on La–YBCO thin film for single flux quantum circuits. The Tb–Mg co-doped $CaSnO_3$ films have been deposited on silica glass and on 100-$SrTiO_3$ for electroluminescence devices. Pulsed laser deposition (PLD) has also been used to prepare pure $SrSnO_3$, Sb-doped $SrSnO_3$, Nd-doped $SrSnO_3$ and Pr-doped $CaSnO_3$ thin films on 100-$SrTiO_3$ [14–16]. Our group has also prepared $SrSnO_3$ films on different substrates at various temperatures using PLD [17]. However, these physical deposition methods (sputtering and PLD) are difficult to industrialize, especially in case of deposition on large area surface, in contrast to other processes based on chemical solution deposition.

Chemical solution deposition (CSD) is indeed very attractive for the synthesis of thin films because it is a low cost process which allows deposition on large area and complex shape substrates. This technique consists of depositing a solution by dip or spin coating followed by a heat treatment to crystallize the desired phase. The advantages of CSD include an accurate stoichiometric control, relatively low synthesis temperatures and the use of a simple equipment which does not require vacuum or atmosphere control [18]. The preparation of perovskite oxide thin films, such as titanates ($SrTiO_3$ [19], (Ba,Sr)TiO_3 [20,21], $PbZr_xTi_{1-x}O_3$ [22]), manganates ($La_{0.67}Sr_{0.33}MnO_3$ [23], $La_{0.7}Pb_{0.3}MnO_3$ [24]), niobates ($KNbO_3$ [25], (K,Na)NbO_3 [26]) and tantalates ($KTa_{1-x}Nb_xO_3$ [18], $KTaO_3$ [27]),

* Corresponding author. Fax: +55 83 32167441.
E-mail address: ieda@quimica.ufpb.br (I.M.G. Santos).

0022-4596/$ - see front matter © 2012 Elsevier Inc. All rights reserved.
http://dx.doi.org/10.1016/j.jssc.2012.11.014

using this method has been previously reported. Various routes can be used to prepare the coating solution such as the sol–gel process based on the chemistry of alkoxides. However, in this case, the metallic precursors are expensive and must be handled in strictly dry atmosphere and solvents. An alternative route to prepare the coating solution is the polymeric precursor method derived from the Pechini process [9,19,20] which presents the advantages to be carried out in aqueous environment and to use relatively cheap precursors.

The aim of this present work is to synthesize $MSnO_3$ (M=Sr and Ca) thin films on different substrates by CSD using the polymeric precursor method. The influence of the network modifier (Ca or Sr) on the temperature of synthesis and also on the structural and microstructural properties of the films was particularly studied.

2. Materials and methods

The synthesis of $MSnO_3$ (M=Sr, Ca) films was performed by CSD based on the polymeric precursor method. This method derived from the Pechini process consists of preparing a polymeric resin where the metallic ions are uniformly dispersed at atomic level. This resin is obtained by complexing metallic cations with citric acid (containing 3 –COOH groups) in an aqueous solution. Then these metal citrates polymerize with ethylene glycol by increasing the temperature. From this resin, powders and thin films can be prepared after a thermal treatment [9,18,19]. The synthesis of $SrSnO_3$ and $CaSnO_3$ polymeric resins has been described in detail elsewhere [9]. Briefly, the citrate solutions were prepared from calcium acetate (Alfa Aesar 99%), strontium nitrate (Alfa Aesar 99%) and tin chloride dehydrate (Alfa Aesar 98%). The ratio [citric acid:cation] was [3:1] in mol and [citric acid:ethylene glycol] was [60:40] in mass. The viscosity of these polymeric resins was then adjusted to approximately 26 cP by addition or evaporation of water and measured using a Brookfield DVIIþ Pro viscometer. The obtained coating solutions were deposited by spin coating at 1000 rpm during 3 s followed by rotation at 4000 rpm during 10 s (Spin Coater model KW-4A Chemat Technology) on the following single crystal substrates: R-sapphire (R-Al_2O_3), C-sapphire (C-Al_2O_3) and 100-$SrTiO_3$ (STO). Only one layer was deposited for each film. Then the wet films were subjected to two thermal treatment cycles as follows: (i) 300 °C for 4 h for organic matter elimination and (ii) 550–700 °C for 2 h for perovskite crystallization. These synthesis conditions allowed for the formation of thin films with a thickness ranging from 220 to 350 nm depending on the deposited material and on the substrate.

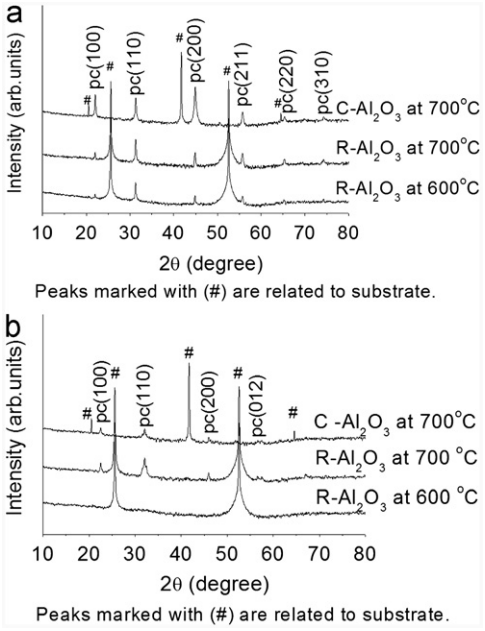

Fig. 1. θ–2θ XRD patterns (log scale) of the thin films deposited on R- and C-Al_2O_3 and heat-treated at 600 and 700 °C for 2 h: $SrSnO_3$ (a) and $CaSnO_3$ (b).

The structural characteristics were analyzed using X-Ray diffraction (XRD). Standard θ–2θ scans were performed with a two-circle Bruker D8 diffractometer using the monochromatized Cu $K_{\alpha 1}$ radiation. The ω-scans (used to evaluate the crystalline quality along the growth direction) and φ-scans (used to study the in-plane orientation) were recorded with a four-circle Bruker D8 Advance diffractometer operating with Cu $K_{\langle\alpha\rangle}$ radiation. Short-range order was evaluated using Raman spectroscopy and photoluminescence (PL). The micro-Raman spectra were obtained with a Witec Alpha 300S Scanning Near-field Optical Microscope with Confocal Raman Imaging Upgrade. A Nd:YAG laser was used with an excitation wavelength of 514 nm and a spectral resolution of 4 cm^{-1}. The PL measurements were performed with a Monospec 27 monochromator (Thermal Jarrel Ash, USA) coupled to a R446 photomultiplier (Hamamatsu, Japan). A 350.7 nm krypton ion laser (Coherent Innova 90K, USA) was used as the excitation source. All of the measurements were performed at room temperature.

Thin film microstructures were observed with a field emission scanning electron microscope (FE-SEM, Jeol 6301-F) which was operated at low voltage, typically 7–9 kV, to limit charge effects and to achieve high resolution without requiring surface metallization. Surface roughness was estimated using an atomic force microscope (AFM, Veeco D3100, Nanoscope V) in tapping mode with a silicon Nano World Pointprobe NCH.

3. Results and discussion

3.1. $MSnO_3$ films grown on sapphire

The θ–2θ XRD patterns of the $MSnO_3$ (M=Sr, Ca) films deposited on C- and R-Al_2O_3 substrates are presented in Fig. 1. For comparison, all of the peaks were indexed relative to a pseudo-cubic cell with a_{pc}=4.034 Å for $SrSnO_3$ and a_{pc}=3.960 Å for $CaSnO_3$ (Table 1).

Pure $SrSnO_3$ and $CaSnO_3$ films were obtained at 700 °C on both substrates. All of the films were polycrystalline, with a small (h00) preferential orientation in the case of $SrSnO_3$ on C-Al_2O_3 (Fig. 1a). Note that a random polycrystalline growth of these materials on C and R-sapphire is not surprising because of the difference of symmetry between the deposited material (perovskite structure) and the substrate (rhombohedral system) and also due to the high

Table 1
Lattice parameters or $SrSnO_3$ and $CaSnO_3$.

	Structure	Lattice parameters (Å)	Parameters in a pseudo-cubic cell (Å)
$SrSnO_3$	Cubic	a=8.0682 (JCPDS 22-1442)	$a_{pc}=a/2=4.034$
$CaSnO_3$	Orthorhombic	a=5.532, b=5.681, c=7.906 (JCPDS 77-1797)	$a_{pc}=[(a+b)\sqrt{2}/2+c/2]/3=3.960$

Table 2
Mismatch values between the films and the substrates with a (1 0 0) film orientation.

Substrate	System	Lattice parameters	Mismatch with $SrSnO_3$	Mismatch with $CaSnO_3$
STO	Cubic	3.905 Å	3.3%	1.4%
R-Al_2O_3	Rhombohedral	4.76 Å// [100] 15.38 Å// $[\bar{1}\,\bar{2}\,1]$	−15% −21%	−17% −23%
C-Al_2O_3	Rhombohedral	4.76 Å// [100]	−15%// [100]	−17%// [100]

mismatch values (Table 2). The peaks were more intense for the $SrSnO_3$ which means that these films crystallized easier than the $CaSnO_3$ ones.

The influence of network modifiers on the crystallization process was also observed at lower temperature (600 °C) where the $SrSnO_3$ film crystallized on R-Al_2O_3, but an amorphous material was obtained for $CaSnO_3$. This difference may be attributed to the $CaSnO_3$ perovskite structure, which has a larger tilt of the octahedra due to the higher covalent character of the Ca^{2+}–O^{2-} bond resulting in poor crystallization [4,5]. The same behavior has been observed for powders synthesized by the polymeric precursor method [9]. In comparison to our previous work on $SrSnO_3$ deposited on R-Al_2O_3 by PLD [17], it is observed that the crystallization of the film occurs at a temperature 100 °C lower when deposition is done using CSD, confirming the interest in this method.

Fig. 2a and b shows the Raman spectra obtained for the $SrSnO_3$ and $CaSnO_3$ films deposited on sapphire. High intensity peaks assigned to the vibrational modes of the sapphire substrate were observed [28,29].

According to the factor group analysis, $CaSnO_3$ perovskites have 24 Raman active modes though some of them are not observed due to low polarizability and overlap with more intense bands [30]. Literature data for the bulk material indicates the presence of a lattice soft mode usually present at 183 cm^{-1}, a Sn–O bending motion normally present at 278 cm^{-1} and a torsional mode usually observed at 354 cm^{-1} [30].

In the present case, the Raman spectra of the $CaSnO_3$ films deposited on R-Al_2O_3 (Fig. 2a) did not show peaks corresponding to the perovskite whereas those deposited on C-Al_2O_3 showed low intensity peaks at 193, 296 and 376 cm^{-1} (Fig. 2b), which indicates that a shift of the peaks occurs. According to the literature, a shift of the Raman peaks relative to the bulk can be attributed to a stress in the films [31]. Ching-Prado et al. [32] have deposited ferroelectric $PbTiO_3$ films on silicon and sapphire by CSD and have observed broader peaks in the Raman spectra with a significant shift to lower frequencies, particularly for the bands in the high frequency range.

For $SrSnO_3$, Singh et al. [33] have assigned the relatively sharp peaks at 90, 223 and 260 cm^{-1} to the Ag modes. According to Moreira et al. [34], the intense peak at 223 cm^{-1} corresponds to the scissor movement of the Sn–O–Sn groups along the *c*-axis while the peak at 252 cm^{-1} is related to the O–Sn–O bending motion within the *ab* plane and the Sn–O–Sn scissoring perpendicular to the *c*-axis. They have also identified different Raman active peaks between 300 and 400 cm^{-1} with vibrations at 302/310 cm^{-1} (superposed), 360 cm^{-1} (weak), 381 and 389 cm^{-1}. The weak peaks located at higher frequencies (observed above 800 cm^{-1}) could be attributed to second-order scattering features resulting from the superposition of different combination modes as proposed by Tarrida et al. [30].

In the present study low intensity peaks assigned to perovskite were observed for $SrSnO_3$ films deposited on both substrates, as shown in Fig. 2(a and b). On R-Al_2O_3, these peaks were present at 236, 282 and 318 cm^{-1}, being observed at 230, 284 and 389 cm^{-1} on C-Al_2O_3. The shifts in the 318 and 389 cm^{-1} modes make their identification more difficult, but they could be related to the peaks observed in the same region by Moreira et al. [34].

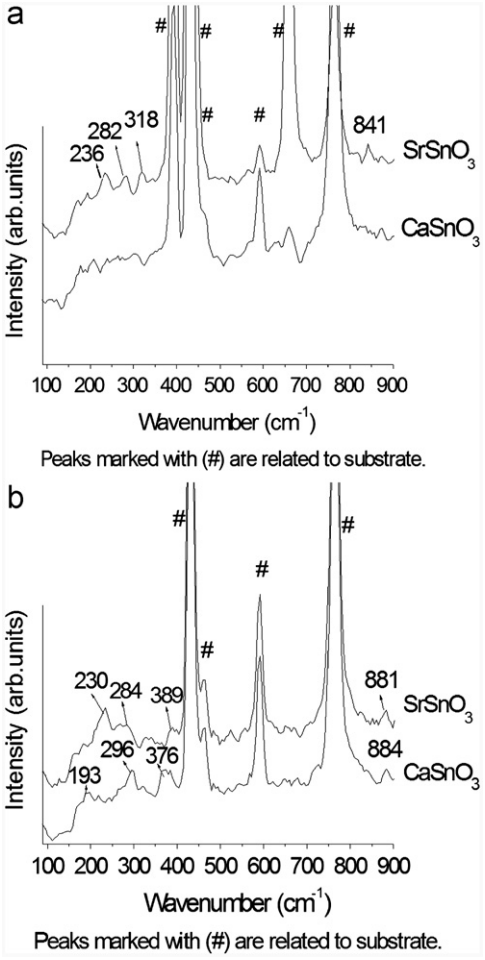

Fig. 2. Micro-Raman spectra of the $SrSnO_3$ and $CaSnO_3$ thin films deposited at 700 °C on (a) R-Al_2O_3 and (b) C-Al_2O_3.

The PL spectra of the films exhibited profiles very similar to the bare substrate (Fig. 3a and b). These results indicated that the emission was mainly due the substrate suggesting that the films were of high short-range order. According to Myhajlenko et al. [35], PL can be used to evaluate crystal defects, impurities, composition, electric fields and film stress. For perovskite films grown by CSD, it has previously been reported that the PL intensity decreases when the films attain a higher short-range order [19,20].

The microstructures of the films synthesized at 600 and 700 °C on R- and C-Al_2O_3 are presented in Figs. 4 and 5. The morphology was strongly influenced by the network modifier (Ca^{2+} or Sr^{2+}) regardless of the sapphire orientation. Homogeneous and crack-free films were obtained for $CaSnO_3$, whereas inhomogeneous microstructures were observed for $SrSnO_3$ films, in particular at 700 °C.

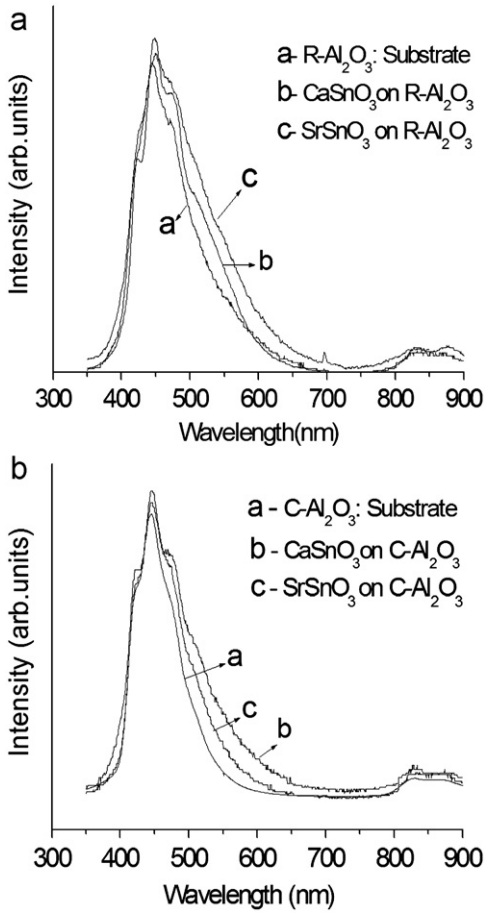

Fig. 3. PL spectra of the $SrSnO_3$ and $CaSnO_3$ thin films deposited at 700 °C on. (a) R-Al_2O_3 and (b) C-Al_2O_3.

According to Deligne et al. [36], the morphology and homogeneity of films obtained by spin-coating are highly dependent on the precursor composition. Hoffmann and Waser [21] have obtained (Ba,Sr)TiO_3 thin films using CSD from solutions based on titanium alkoxide and have evaluated the influence of precursor chemistry and deposition process conditions on the morphology. Precursors with different decomposition temperatures have been used for Ba and Sr and different crystallization behaviors have been observed which led to different morphologies. This same type of influence has been observed by Malic et al. [37] for $PbTiO_3$ thin films also obtained from solutions based on titanium alkoxide. However, Giraldi et al. [38] have studied the chemical synthesis of ZnO particles and have observed that when the polymeric precursor method is used, the influence of the precursor composition becomes much less pronounced probably due to the formation of metallic citrate in the initial stages of the synthesis which practically overrides the effect of the any other counter ion. In the present case, we can also consider the previous studies of our research group on bulk $CaSnO_3$ obtained by the polymeric precursor method [39]. The thermogravimetric curves for the pyrolysed polymeric precursors obtained from calcium acetate or calcium nitrate have the same final decomposition temperature (around 750 °C). In another study [9], the crystallization of $SrSnO_3$ and $CaSnO_3$ using calcium acetate and strontium nitrate as precursors was evaluated and carbonates were found in both syntheses, without other intermediate phases. In this sense, the use of nitrate or acetate does not change the decomposition and may not influence the crystallization.

We believe that the difference in the morphologies of $SrSnO_3$ and $CaSnO_3$ films are assigned to the different behavior of the two materials during the crystallization process, as previously observed by XRD. For $SrSnO_3$ films, nucleation starts near 600 °C, thus the grain growth process becomes predominant at higher temperatures (700 °C) which could lead to the coalescence of the grains and to a heterogeneous microstructure. For $CaSnO_3$ films, the crystallization begins at higher temperature (650 °C) and thus it is probably still governed by a nucleation process at 700 °C. As a consequence, $CaSnO_3$ presents at this temperature a homogeneous microstructure, composed by small grains. The effect of nucleation/grain growth processes on film morphology is also quite dependent of the deposition technique. For example, $SrSnO_3$ thin films deposited at 700 °C on R-Al_2O_3 by PLD have presented a homogeneous surface [17], due to the fact that in PLD films crystallization occurs directly from the vapor phase on the heated substrate whereas in the case of CSD, the crystallites form from an amorphous phase, the crystallization process is slower and usually begins at lower temperature.

3.2. $MSnO_3$ film grown on STO

The influence of the heat treatment temperature on the $MSnO_3$ crystallization process was also investigated for thin films deposited on STO substrates (Fig. 6). The $SrSnO_3$ films prepared at different temperatures exhibited (h 0 0) preferential growth except for the film annealed at 550 °C, which only exhibited very weak (1 1 0) and (1 1 1) peaks indicating that the crystallization began around this temperature (Fig. 6a). For $CaSnO_3$, (h 0 0) preferential growth was only observed at and above 650 °C, while the sample prepared at 600 °C exhibited very weak (1 1 1) peak suggesting that the crystallization had just begun (Fig. 6b). These results suggested that the crystallization process was easier for $SrSnO_3$, which is in agreement with previous results obtained on sapphire.

The ω-scan performed around the pc(2 0 0) $SrSnO_3$ peak for the film grown at 600 °C confirmed a high crystalline quality of the out-of-plane growth with $\Delta\omega = 0.46°$ (inset of Fig. 6a). The temperature increase did not result in a meaningful influence on the crystalline quality: $\Delta\omega = 0.62°$ and 0.60° (inset of Fig. 6b) at 650 °C and 700 °C, respectively. The in-plane investigation revealed an epitaxial growth for these films as shown by the φ-scans obtained for $SrSnO_3$ prepared at 600 °C and 700 °C (Fig. 7a and b). The epitaxial growth is favoured by the low mismatch value between the film and the substrate (Table 2) in addition to similar crystalline structures.

The same behavior was observed for $CaSnO_3$, which crystallization started at a temperature 50 °C higher. Epitaxial growth was confirmed for the films synthesized at 650 °C and 700 °C. As an example, Fig. 7c shows the φ-scan of the sample treated at 700 °C. The ω-scan performed around the pc(1 0 0) peak of this same film confirmed the good quality of the epitaxy with $\Delta\omega = 1°$ (inset Fig. 6c). The unusual shape observed for this ω-scan pattern can be related to different structural qualities in the film (from the interface towards the surface) [40] or to a superposition of the contributions from the STO substrate (FWHM of approximately 0.06°) and from the film. In the present study, this superposition cannot be excluded because of the close positions of the two peaks of the $CaSnO_3$ and STO in the θ–2θ XRD patterns. This hypothesis is also supported by a study performed by our group on $Ca_{1-x}Sr_xSnO_3$ (x=0, 0.25, 0.50, 0.75 and 1) thin films prepared using PLD or CSD on STO. In that case, the unusual shape of the ω-scan pattern was only obtained for x=0, i.e., for the $CaSnO_3$ composition for which the positions of the two peaks of the film and the substrate are closer in the θ–2θ XRD patterns compared to the other compositions.

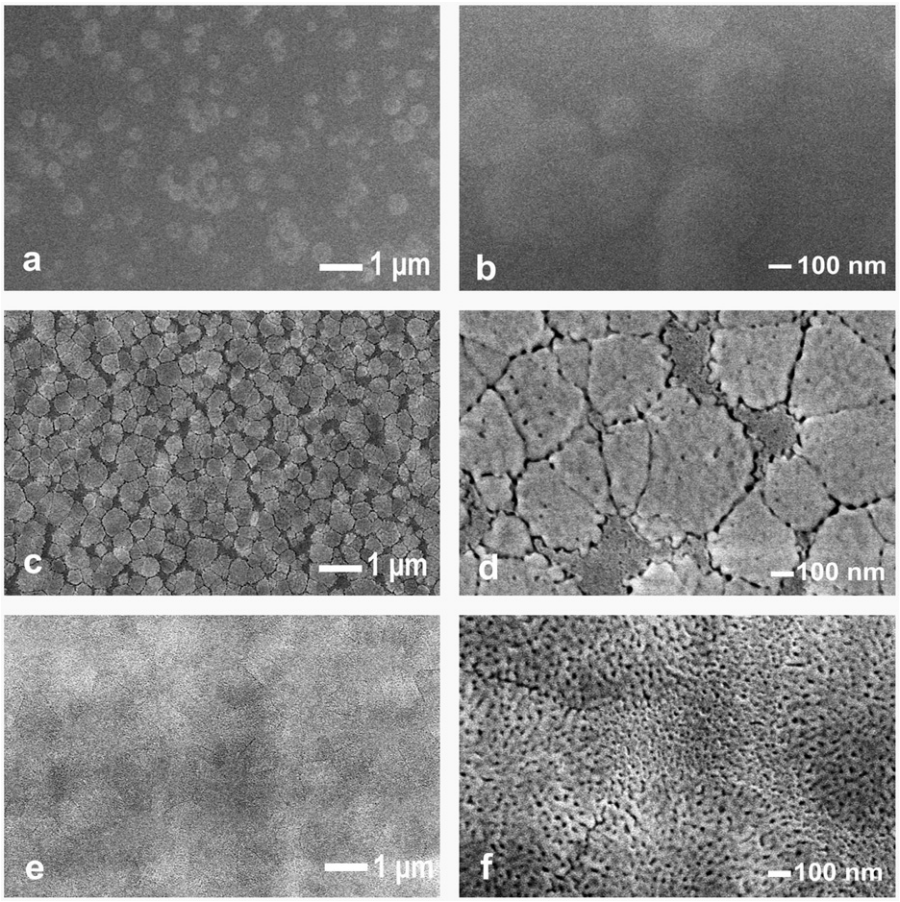

Fig. 4. FE–SEM images of the thin films synthesized on R-sapphire: (a) and (b) $SrSnO_3$ at 600 °C; (c) and (d) $SrSnO_3$ at 700 °C; (e) and (f) $CaSnO_3$ at 700 °C.

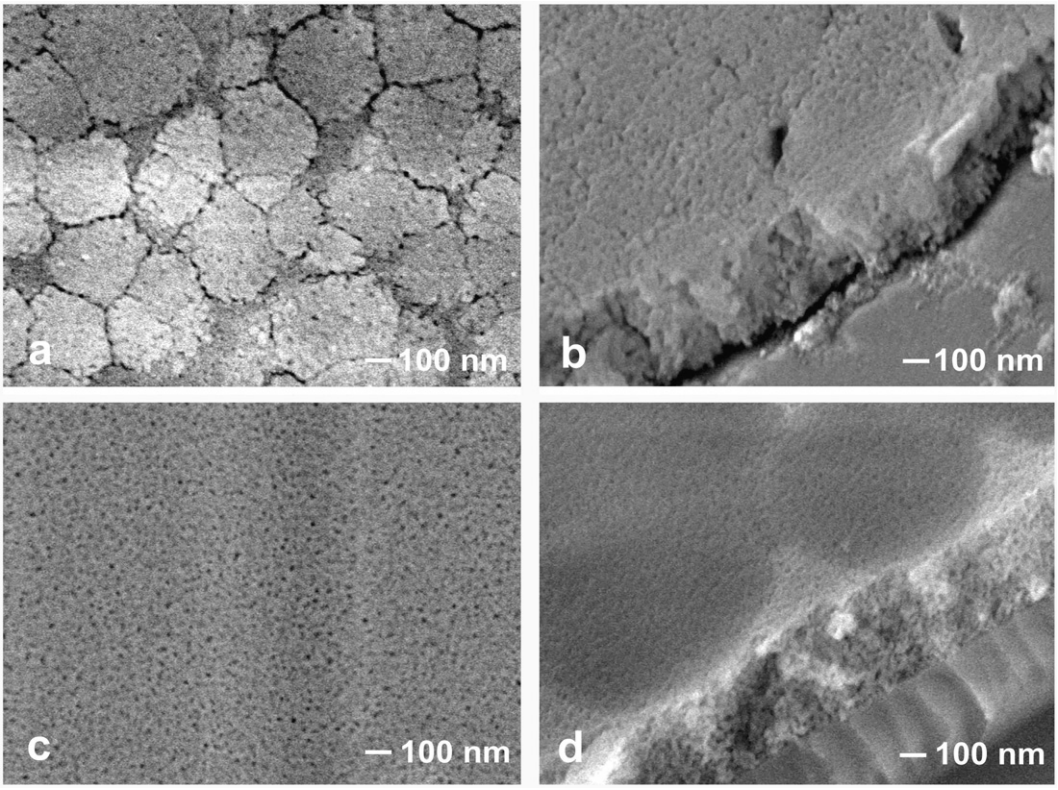

Fig. 5. FE–SEM images of the thin films synthesized at 700 °C on C-Al_2O_3 substrate: (a) and (b) $SrSnO_3$; (c) and (d) $CaSnO_3$.

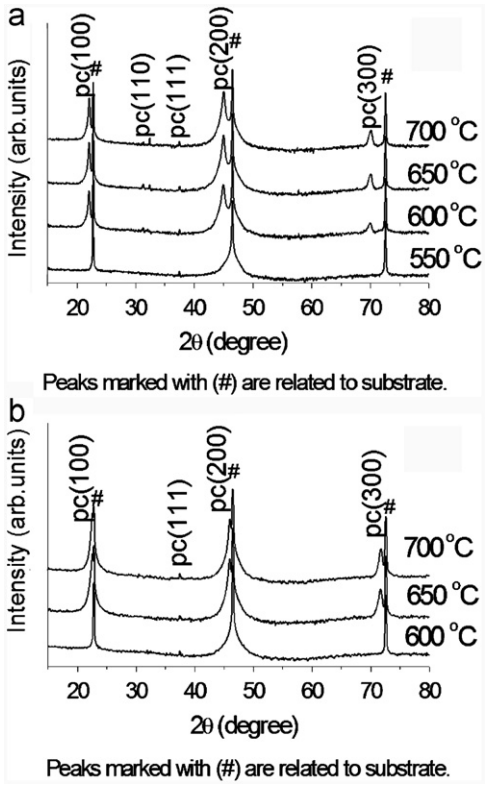

Fig. 6. θ–2θ XRD patterns (log scale) of the thin films deposited on STO and heat-treated at different temperatures for 2 h: $SrSnO_3$ (a) and $CaSnO_3$ (b).

Our research group reported the preparation of $SrSnO_3$ thin films by PLD on STO with thicknesses similar to the values obtained in the present work [17]. It should be noted that a similar crystalline quality was observed for both deposition methods (PLD and CSD). The epitaxial growth of Sb-doped and Nd-doped $SrSnO_3$ by PLD on STO at 600 °C has also been previously reported [14,16]. For these films, a higher crystalline quality was obtained compared to the present work, which could be attributed to the lower film thicknesses or to a possible doping effect. Thin films of $CaSnO_3$:Tb–Mg were deposited by RF sputtering on STO substrates, but the nature of the film growth was not investigated [13]. Ueda et al. [15] synthesized $CaSnO_3$:Pr on STO by PLD and obtained high quality epitaxy consistent with our results.

In this work, the films deposited on STO were also investigated by Raman spectroscopy. However, the identification of vibrational modes related to the films was difficult due to the presence of broad bands assigned to the second-order spectra of cubic $SrTiO_3$, which was used as the substrate [41,42]. This same difficulty was observed for $PbTiO_3$ films deposited on $SrTiO_3$ and on $KTaO_3$ [43].

PL spectra of films deposited on the STO substrate exhibited an emission band with a profile similar to the substrate, but with a higher intensity especially for the $CaSnO_3$ thin film (Fig. 8).

The photoluminescence for $SrSnO_3$ was reported by Bohnemann et al. [10] for powders synthesized from $SrSn(OH)_6$ precursors calcined using conventional or microwave furnaces. The highest PL emission was observed for samples obtained by microwave-assisted calcination due to the presence of medium-range disorder in the structures. Park et al. [44] synthesized $SrZrO_3$ and $SrHfO_3$ perovskites by solid state reaction. The authors associated the photoluminescence with the degree of order-disorder in the structure which alters the localized states existing in the bandgap. PL was also associated with defects in epitaxial Si-doped ZnO thin films deposited on Zn_2SiO_4 by vapor deposition [45]. Therefore, PL emission is a

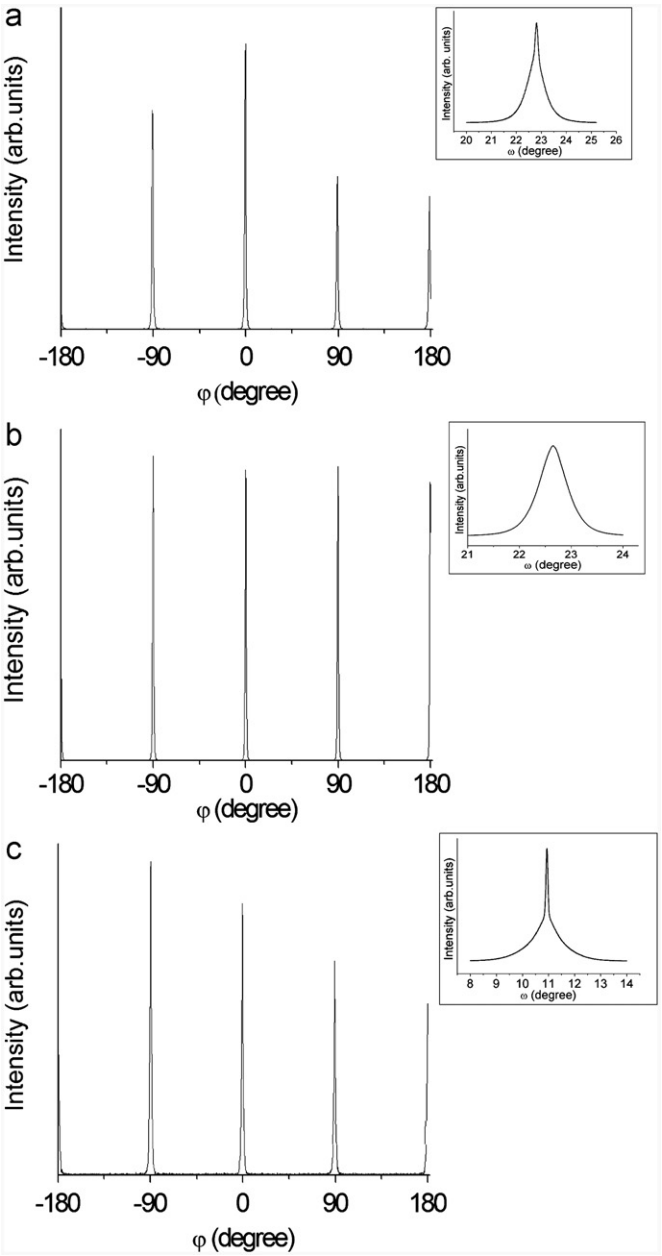

Fig. 7. φ-scan of the pc(1 1 0) reflection and ω-scan (in inset) of the thin films synthesized on STO: (a) $SrSnO_3$ at 600 °C; (b) $SrSnO_3$ at 700 °C; (c) $CaSnO_3$ at 700 °C. The ω-scans were performed on the pc(2 0 0) $SrSnO_3$ peak and on the pc(1 0 0) $CaSnO_3$ peak.

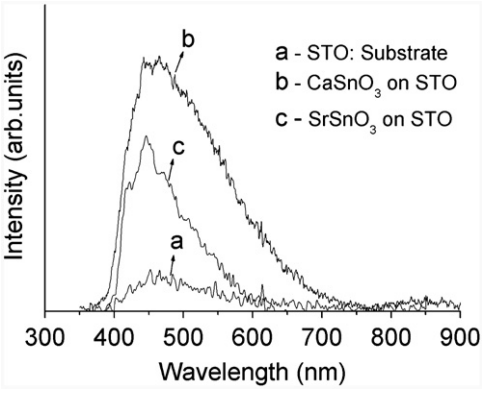

Fig. 8. PL spectra of the $SrSnO_3$ and $CaSnO_3$ thin films deposited on STO at 700 °C.

good approach for identifying the presence of short or medium-range disorder in crystalline structures.

For $CaSnO_3$, photoluminescence was observed by Ueda et al. [15] for Pr-doped epitaxial thin films deposited on STO by PLD. In this case, emission arised from praseodymium occupying well-ordered sites. The as-grown epitaxial films contained defects (i.e., oxygen vacancies) which led to low PL associated with the electronic transitions of Pr^{3+}. Post-annealing in air reduced the defects and increased the crystallinity considerably, resulting in an enhanced radiative decay process.

In the present case, photoluminescence seems to be related to the type of growth. As indicated by XRD results, the $MSnO_3$ thin films are epitaxial on STO. A short-range disorder may occur at the interface film/substrate in order to enable the epitaxial growth. $SrSnO_3$ and $CaSnO_3$ are characterized by an inclination among octahedra due to the covalent character of the modifier cations (Sr^{2+} or Ca^{2+}) [4,5]. The structure of STO substrate is cubic without inclination among octahedra. The short disorder would correspond to a change in the tilt of the SnO_6 octahedra in order to attain a higher alignment with the TiO_6 octahedra of the substrate at the interface.

Orhan et al. [19] have studied the photoluminescence in $SrTiO_3$ thin films associated to theoretical calculations. They have evaluated the influence of different coordinations around Ti^{4+} in the same crystal structures which simulated the short-range disorder and have observed that different clusters present different net cluster charges which induce the formation of a charge gradient – a dipole – in the lattice. This gradient is responsible for the trapping of holes in new localized electronic levels, leading to photoluminescence. We believe that in the present case, when one moves away from the interface, the influence of the substrate decreases which leads to a decrease of the short-range disorder. As a consequence, dipoles are formed between the well-ordered SnO_6 octahedra (far from the interface) and the disordered ones

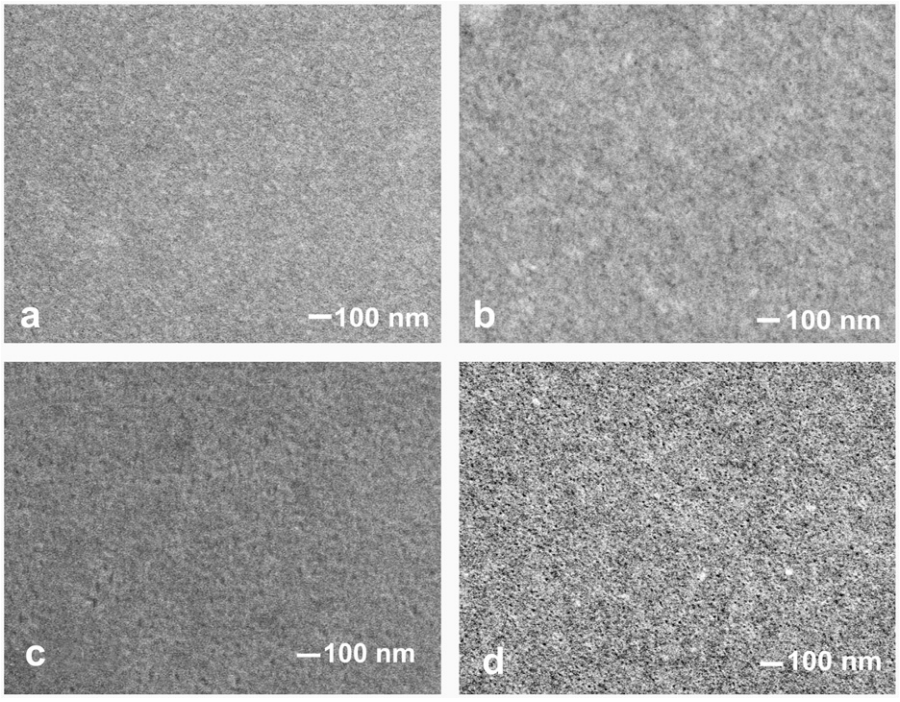

Fig. 9. FE-SEM images of the thin films synthesized on the STO substrate and heat-treated at different temperatures: $SrSnO_3$ (a) at 600 °C and (b) 700 °C and $CaSnO_3$ (c) at 600 °C and (d) 700 °C.

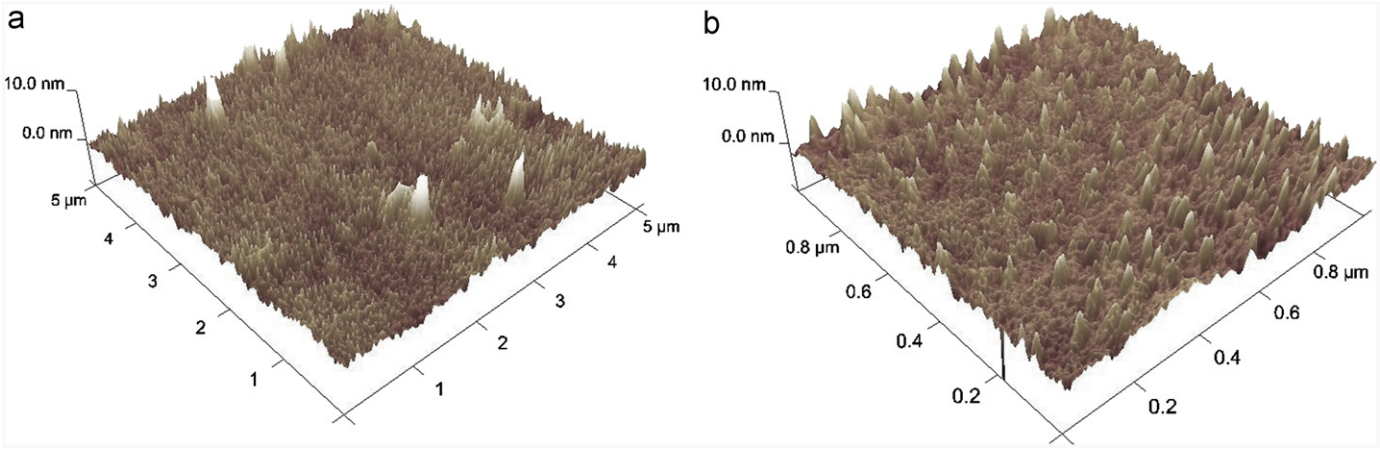

Fig. 10. AFM images of the $SrSnO_3$ thin film synthesized at 600 °C on STO. (a) $5 \times 5\ \mu m^2$ analyzed area; (b) $1 \times 1\ \mu m^2$ analyzed area.

(located at the interface) which lead to the variation in the photoluminescence comparing to the emission from substrate. Since $CaSnO_3$ exhibits a higher inclination among octahedra compared to $SrSnO_3$, a higher short-range disorder at the interface would be necessary to attain the epitaxial growth which could explain the higher PL intensity observed for this material.

Fig. 9 displays FE–SEM images for the $MSnO_3$ grown on STO substrates at 600 and 700 °C. All of the films exhibited similar crack-free homogeneous microstructures. AFM images of all of the films revealed very smooth surfaces as shown for $SrSnO_3$ annealed at 600 °C in Fig. 10 (R_{RMS}=1.1 nm for $1\times1\ \mu m^2$ analyzed area and R_{RMS}=1.2 nm for $5\times5\ \mu m^2$ area). As previously observed on sapphire, the deposition method strongly influences the film microstructure with smaller R_{RMS} values obtained with the CSD method [17].

4. Conclusions

$CaSnO_3$ and $SrSnO_3$ thin films were successfully obtained by CSD at low temperature on STO, R- and C-Al_2O_3. For films deposited on STO at 600 °C, epitaxy was only observed for the $SrSnO_3$ films, whereas the $CaSnO_3$ films had just begun to crystallize, becoming epitaxial at 650 °C. In contrast, random polycrystalline $SrSnO_3$ and $CaSnO_3$ films were obtained on R- and C-Al_2O_3, with a small (h00) preferential orientation for $SrSnO_3$ film deposited on C-Al_2O_3. Regardless of the substrate, crystallization of $SrSnO_3$ films always occurred at a lower temperature, which could be related to the smaller tilt of the octahedral in this material when compared to $CaSnO_3$. Furthermore, the epitaxial growth induced a short-range disorder which led to a variation of the photoluminescence compared to the emission from the substrate. Indeed, PL was only observed in films grown on STO, while no emission assigned to the films was observed for depositions on sapphire. With respect to the microstructure, the deposition on sapphire promoted a heterogeneous morphology for the $SrSnO_3$, while all of the other films were homogeneous.

Acknowledgment

The authors acknowledge the French-Brazilian doctoral college, CAPES-COFECUB (Project 644/09), INCT/CNPq/MCT and PROINFRA/FINEP/MCT for financial support, J. Le Lannic for SEM images at CMEBA of University of Rennes, S. Ollivier for AFM images, J.C. Sangleboeuf and T. Rouxel for the access to the AFM equipment and A. Gallembeck for micro-Raman spectra at CETENE/MCT (Centro de Tecnologias Estratégicas do Nordeste—Brazil).

References

[1] M.K. Mahapatra, P. Singh, D. Kumar, O. Parkash, Adv. Appl. Ceram. 105 (2006) 280–284.
[2] W. Zhang, J. Tang, J. Ye, J. Mater. Res. 22 (2007) 1859–1871.
[3] N. Sharma, K.M. Shaju, G.V.S. Rao, B.V.R. Chowdari, Electrochem. Commun. 4 (2002) 947–952.
[4] H. Mizoguchi, H.W. Eng, P.M. Woodward, Inorg. Chem. 43 (2004) 1667–1680.
[5] E.H. Mountstevens, J.P. Attfield, S.A.T. Redfern, J. Phys. 15 (2003) 8315–8326.
[6] A.M. Azad, L. Liew, W. Shyan, P.T. Yen, J. Alloys Compd. 282 (1999) 109–124.
[7] A.M. Azad, M. Hashim, S. Baptist, A. Badri, A.U. Haq, J. Mater. Sci. 35 (2000) 5475–5483.
[8] Z. Lu, J. Liu, J. Tang, Y. Li, Inorg. Chem. Commun. 7 (2004) 731–733.
[9] M.C.F. Alves, S.C. Souza, H.H.S. Lima, M.R. Nascimento, M.R.S. Silva, J.W.M. Espinosa, S.J.G. Lima, E. Longo, P.S. Pizani, L.E.B. Soledade, A.G. Souza, I.M.G. Santos, J. Alloys Compd. 476 (2009) 507–512.
[10] J. Bohnemann, R. Libanori, M.L. Moreira, E. Longo, Chem. Eng. J. 155 (2009) 905–909.
[11] C.P. Udawatte, M. Kakihana, M. Yoshimura, Solid State Ionics 128 (2000) 217–226.
[12] H. Wakana, A. Kamitani, S. Adachi, K. Nakayama, Y. Ishimaru, Y. Tarutani, K. Tanabe, Phys. Chem. 426 (2005) 1495–1501.
[13] K. Ueda, Y. Shimizu, Thin Solid Films 518 (2010) 3063–3066.
[14] Q.Z. Liu, H.F. Wang, F. Chen, W. Wenbin, J. Appl. Phys. 103 (2008) 093709.
[15] K. Ueda, T. Maeda, K. Nakayashiki, K. Goto, Y. Nakachi, H. Takashima, K. Kajihara, H. Hosono, Appl. Phys. Express 1 (2008) 015003.
[16] Q. Liu, J. Dai, X. Zhang, G. Zhu, Z. Liu, G. Ding, Thin Solid Films 519 (2011) 6059–6063.
[17] M.C.F. Alves, S. Boursicot, S. Ollivier, V. Bouquet, S. Deputier, A. Perrin, I.T. Weber, A.G. Souza, I.M.G. Santos, M. Guilloux-Viry, Thin Solid Films 510 (2010) 614–618.
[18] Q. Simon, V. Bouquet, A. Perrin, M. Guilloux-Viry, Solid State Sci. 11 (2009) 91–95.
[19] E. Orhan, F.M. Pontes, M.A. Santos, E.R. Leite, A. Beltrán, J. Andrés, T.M. Boschi, P.S. Pizani, J.A. Varela, C.A. Taft, E. Longo, J. Phys. Chem. B 108 (2004) 9221–9227.
[20] E. Longo, E. Orhan, F.M. Pontes, C.D. Pinheiro, E.R. Leite, J.A. Varela, P.S. Pizani, T.M. Boschi, F. Lanciotti, A. Beltrán, J. Andrés, Phys. Rev. B 69 (2004) 125115.
[21] S. Hoffmann, R. Waser, J. Europ., Ceram. Soc. 19 (1999) 1339–1343.
[22] T. Miyazaki, T. Imai, N. Wakiya, N. Sakamoto, D. Fu, H. Suzuki, Mater. Sci. Eng. B 173 (2010) 89–93.
[23] S.Y. Kuo, C.S. Chen, T.Y. Tseng, S.C. Chang, W.F. Hsieh, J. Appl. Phys. 92 (2002) 1868–1872.
[24] P.S. Solanki, R.R. Doshi, U.C. Khachar, R.J. Choudhary, D.G. Kuberkar, Mater. Res. Bull. 46 (2011) 1118–1123.
[25] T. Ohno, M. Fujimoto, T. Ota, M. Fuji, M. Takahashi, H. Suzuki, J. Europ., Ceram. Soc. 26 (2006) 2143–2146.
[26] C. Schroeter, B. Wessler, L.M. Eng, J. Europ., Ceram. Soc. 27 (2007) 3785–3788.
[27] I.T. Weber, N. Audebrand, V. Bouquet, M. Guilloux-Viry, A. Perrin, Solid State Sci. 8 (2006) 606–612.
[28] A. Aminzadeh, H. Sarikhani-fard, Spectrochim. Acta, Part A 55 (1999) 1421–1425.
[29] M. Kadleíková, J. Breza, M. Veselý, Microelectron. J. 32 (2001) 955–958.
[30] M. Tarrida, H. Larguem, M. Madon, Phys. Chem. Miner. 36 (2009) 403–413.
[31] P.S. Dobal, R.S. Katiyar, J. Raman Spectrosc. 33 (2002) 405–423.
[32] E. Ching-Prado, J. Cordero, R.S. Katiyar, A.S. Bhalla, J. Vac. Sci. Technol., A 14 (1996) 762–768.
[33] M.K. Singh, J.W. Hong, N.K. Karan, H.M. Jang, R.S. Katiyar, S.A.T. Redfern, J.F. Scott, J. Phys.: Condens. Matter 22 (2010) 095901.
[34] E. Moreira, J.M. Henriques, D.L. Azevedo, E.W.S. Caetano, V.N. Freire, E.L. Albuquerque, J. Solid State Chem. 184 (2011) 921–928.
[35] S. Myhajlenko, A. Bell, F. Ponce, J.L. Edwards Jr., Y. Wei, B. Craigo, D. Convey, H. Li, R. Liu, J. Kulik, J. Appl. Phys. 97 (2005) 014101.
[36] N. Deligne, J. Lamme, M. Devillers, Europ. J. Inorg. Chem. 23 (2011) 3461–3468.
[37] B. Malic, J. Cilensek, M. Mandeljc, M. Kosec, Acta Chim. Slov. 52 (2005) 259–263.
[38] T.R. Giraldi, G.V.F. Santos, V.R. de Mendonca, C. Ribeiro, I.T. Weber, Mater. Chem. Phys. 136 (2012) 505–511.
[39] M.C.F. Alves, S.C. Souza, S.J.G. Lima, E. Longo, A.G. Souza1, I.M.G. Santos, J. Therm. Anal. Calorim. 87 (2007) 763–766.
[40] X. Castel, M. Guilloux-Viry, A. Perrin, J. Lesueur, F. Lalu, J. Cryst. Growth 187 (1998) 211–220.
[41] W.G. Nilsen, J.G. Skinner, J. Chem. Phys. 48 (1968) 2240–2248.
[42] P. Ranson, R. Ouillon, J.-P. Pinan-Lucarre, P. Pruzan, S.K. Mishra, R. Ranjan, D. Pandey, J. Raman Spectrosc. 36 (2005) 898–911.
[43] L. Sun, Y.F. Chen, L. He, C.-Z. Ge, D.-S. Ding, T. Yu, M.-S. Zhang, Phys. Rev. B 55 (1997) 12218.
[44] J.W. Park, D.J. Lee, D.H. Kim, Y.S. Le, J. Korean. Phys. Soc. 58 (2011) 316–320.
[45] B.C. Cheng, X.M. Yu, H.J. Liu, Z.G. Wang, J. Phys. Chem. C 112 (2008) 16312–16317.